Predicted and experimental crystal structures of ethyl-*tert*-butyl ether

**Sonja M. Hammer, Edith Alig,
Lothar Fink and Martin U.
Schmidt***

Institute of Inorganic and Analytical Chemistry,
Goethe University, Max-von-Laue-Strasse 7, D-
60438 Frankfurt am Main, Germany

Correspondence e-mail:
m.schmidt@chemie.uni-frankfurt.de

Possible crystal structures of ethyl-*tert*-butyl ether (ETBE) were predicted by global lattice-energy minimizations using the force-field approach. 33 structures were found within an energy range of 2 kJ mol^{-1} above the global minimum. Low-temperature crystallization experiments were carried out at 80–160 K. The crystal structure was determined from X-ray powder data. ETBE crystallizes in $C2/m$, $Z = 4$, with molecules on mirror planes. The ETBE molecule adopts a *trans* conformation with a $(CH_3)_3C\!-\!O\!-\!C\!-\!C$ torsion angle of 180°. The experimental structure corresponds with high accuracy to the predicted structure with energy rank 2, which has an energy of 0.54 kJ mol^{-1} above the global minimum and is the most dense low-energy structure. In some crystallization experiments a second polymorph was observed, but the quality of the powder data did not allow the determination of the crystal structure. Possibilities and limitations are discussed for solving crystal structures from powder diffraction data by real-space methods and lattice-energy minimizations.

1. Introduction

Ethyl-*tert*-butyl ether (ETBE, Fig. 1) is a gasoline additive which acts as an octane booster (anti-knock agent). At room temperature ETBE is a highly inflammable volatile liquid (m.p. 179 K, b.p. 346 K). It is not toxic but has a bad smell and very low odour and flavour thresholds of 1 and 2 µg L^{-1} (van Wezel *et al.*, 2009). Therefore, small concentrations of ETBE would make ground water undrinkable; the biodegradation is slow, which exacerbates the problem.

Industrially ETBE is synthesized from isobutene and ethanol. The use of bioethanol leads to 'bio-ETBE', which is considered as a biofuel. According to the Directive 2003/30/EC of the European Parliament, from 2011 onwards all fuels placed on the European markets must contain at least 5.75% of biofuels.

As a result of these and other similar regulations, ETBE has started to replace the corresponding methyl derivate, methyl-*tert*-butyl ether (MTBE), which has similar properties to
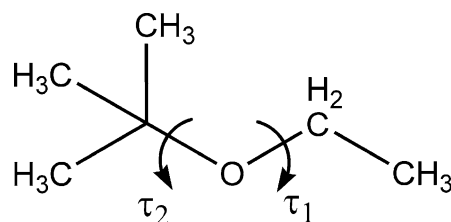
Figure 1
Ethyl-*tert*-butyl ether. The arrows indicate the main intramolecular degrees of freedom (torsion angles).

ETBE and has been produced in quantities of around 20 million tons per year (EFOA, 2005).

Despite the industrial importance of ETBE, no crystal structure has previously been reported. Until now, only the crystal structures of MTBE (Slovokhotov *et al.*, 1984) and *tert*-butanol (Steininger *et al.*, 1989), which is the degradation product of MTBE and ETBE in the atmosphere, have been known.

The molecular structure of ETBE in the gas phase has been investigated by rotational spectroscopy (Suenram *et al.*, 1997) and electron diffraction (Egawa *et al.*, 1993; see Table 1). The molecule is flexible with two main torsion angles, τ_1 and τ_2 (see Fig. 1). According to gas-phase electron diffraction studies ETBE exists in a conformational equilibrium of two forms, *trans* ($\tau_1 = \tau_2 = 180°$) and skew ($\tau_1 \simeq 128°$, $\tau_2 \simeq 179°$), in the ratio $70{:}30 \pm 24\%$ (Egawa *et al.*, 1993). The rotational spectra indicate that the *trans* form is the lowest-energy conformation (Suenram *et al.*, 1997). To our knowledge the structure of ETBE in the solid state has not yet been investigated.

Here we present a crystal-structure prediction for ETBE. Additionally we performed low-temperature crystallizations and determined the crystal structure of one polymorph of ETBE from X-ray powder data.

2. Crystal-structure prediction

2.1. Method

Possible crystal structures of ETBE were predicted by global lattice-energy minimization with force-field methods using the program *CRYSCA* (Schmidt & Kalkhof, 2002).

The molecular structure of ETBE was taken from force-field calculations with the Dreiding/X6 force field (Mayo *et al.*, 1990). *Ab initio* calculations on the HF/6-31G(d,p) level gave a similar geometry. Both structures were in good agreement with experimental results from rotational spectroscopy and gas-phase electron diffraction (see Table 1).

For the lattice-energy minimizations with *CRYSCA* the torsion angles τ_1 and τ_2 were allowed to vary without constraints, whereas all bond lengths and angles were kept fixed. The four methyl groups were each constrained to be in the staggered conformation.

For the rotation around τ_1 a torsional potential was calculated by *ab initio* methods on the HF/6-31G(d,p) level using the *GAUSSIAN*03 package (Frisch *et al.*, 2004). The potential was fitted by a six-term cosine series for use in *CRYSCA*. Similarly, for τ_2 another six-term cosine series was used, which had been developed for alkyl chains (Kalkhof, 2002). Details for both the cosine series are given in the supplementary material (formula S1).[1]

---

[1] Supplementary data for this paper are available from the IUCr electronic archives (Reference: OG5046). Services for accessing these data are described at the back of the journal.

Table 1
Molecular geometry (Å, °) of ETBE.

	DREIDING/X6	HF/6-31 G(d,p)	Rotational spectroscopy (Suenram *et al.*, 1997)	Gas-phase electron diffraction (Egawa *et al.*, 1993)
C2—C3	1.547	1.527	1.495 (6)	1.530 (2)
C2—C4	1.551	1.532	1.565 (6)	1.534 (2)
C2—C5	1.551	1.532	1.565 (6)	1.534 (2)
C2—O1	1.445	1.417	1.417 (16)	1.436 (3)
C6—O1	1.438	1.399	1.423 (4)	1.422 (3)
C6—C7	1.534	1.517	1.512 (3)	1.524 (2)
C3—C2—O1	104.4	103.7	105.9 (6)	
C4—C2—O1	112.2	111.4	110.5 (6)	
C5—C2—O1	112.2	111.0	110.5 (6)	
C3—C2—C4	108.6	109.9	110.7 (4)	111.1 (5)
C3—C2—C5	108.6	109.9	110.7 (4)	111.1 (5)
C4—C2—C5	110.7	110.8	108.4 (6)	
C2—O1—C6	117.7	120.3	119.4 (8)	119.9 (12)
O1—C6—C7	108.5	107.6	108.2 (3)	109.3 (15)

In *CRYSCA* the energy is calculated using the formula

$$E = \tfrac{1}{2} \sum_i \sum_j \left(-A_{ij} r_{ij}^{-6} + B_{ij} e^{-C_{ij} r_{ij}} + \frac{1}{4\pi\varepsilon_0} \frac{q_i q_j}{r_{ij}} \right) + E_{\mathrm{intramol}},$$

(1)

where r_{ij} is the interatomic distance between atoms i and j; A_{ij}, B_{ij} and C_{ij} are potential parameters; q_i and q_j are atomic charges; E_{intramol} is the intramolecular energy.

The Dreiding/X6 parameterization was used for van der Waals parameters A, B and C with a cut-off radius of 20 Å. Atomic point charges were calculated using the method of Gasteiger & Marsili (1980). The summation for the electrostatic energy included $7 \times 7 \times 7$ unit cells. It was extended to 21 unit cells in the corresponding directions for polar axes (*e.g.* $21 \times 7 \times 21$ unit cells for *Cc*).

The crystal structure predictions were performed in space groups which are frequent for molecular crystals: $P1$ ($Z = 1$), $P\bar{1}$ ($Z = 2$), $P2_1$ ($Z = 2$), Cc ($Z = 4$), $C2$ ($Z = 4$), $C2/c$ ($Z = 8$), $P2_1/c$ ($Z = 4$), $P2_12_12_1$ ($Z = 4$), $Pna2_1$ ($Z = 4$), $Pca2_1$ ($Z = 4$) and $Pbca$ ($Z = 8$). In all cases the asymmetric unit contained one molecule on a general position. Since the ETBE molecule may have mirror symmetry, supergroups with molecules situated on crystallographic mirror planes could be reached in the course of the optimization where the molecules are situated on crystallographic mirror planes. For example, the symmetry $P2_1/m$, $Z = 2$ (which is the most frequent space group for molecules on mirror planes), can be reached from $P\bar{1}$, $Z = 2$, $P2_1$, $Z = 2$, or even from $P2_1/c$, $Z = 4$.

For each space group the calculation was started with a set of 10 000 different randomly generated structures having random starting values (within sensible ranges) for τ_1, τ_2, the lattice parameters, and the position and orientation of the molecule. After optimization the structures were sorted according to energy. All the low-energy structures were found several times from different starting points, indicating that the calculation runs were complete and no other low-energy structures were missed.

Table 2
Predicted low-energy structures.

Rank	E (kJ mol^{-1})	Space group	Z	a (Å)	b (Å)	c (Å)	α (°)	β (°)	γ (°)	τ_1 (°)	τ_2 (°)	Density (g cm^{-3})
1	−79.253	$P2_12_12_1$	4	8.5271	8.6360	9.5368	90	90	90	177.1	177.2	0.967
2	−78.712	$C2/m$	4	14.7235	7.8836	6.1684	90	102.699	90	180.0	180.0	0.972
3	−78.568	$P2_12_12_1$	4	7.2271	9.8420	9.9161	90	90	90	177.8	179.2	0.963
4	−78.250	$Pnma$	4	6.1457	7.9315	14.4113	90	90	90	180.0	180.0	0.967
5	−78.129	Cc	4	9.8208	9.7558	8.0684	90	111.570	90	179.2	179.2	0.944
6	−77.997	$P2_1/c$	4	5.1943	16.6606	8.2435	90	92.440	90	174.1	173.2	0.953
7	−77.955	$P2_12_12_1$	4	7.8137	8.0388	11.2982	90	90	90	171.1	170.0	0.957
8	−77.820	$P2_1/c$	4	6.1274	14.0987	9.4241	90	119.330	90	179.8	174.8	0.957
9	−77.805	$Pca2_1$	4	16.7205	5.1990	8.2231	90	90	90	174.5	173.3	0.950
10	−77.786	$P\bar{1}$	4	5.2228	8.7897	15.5584	89.309	89.237	84.216	170.6	174.6	0.956
11	−77.762	$P2_1$	4	9.3824	8.5784	9.2719	90	105.623	90	174.3	179.8	0.945
12	−77.727	$Pbca$	8	8.6847	15.1513	10.9207	90	90	90	173.4	178.2	0.948
13	−77.694	$P2_12_12_1$	4	7.8510	8.9454	10.1930	90	90	90	175.4	176.0	0.948
14	−77.685	$P2_1/c$	4	8.4936	10.9441	8.6739	90	116.903	90	173.7	178.4	0.944
15	−77.623	$P2_1/c$	4	5.2680	7.2894	18.7355	90	97.267	90	175.5	176.8	0.951
16	−77.572	$P2_1$	4	9.5518	7.5091	9.9320	90	91.833	90	175.6	175.5	0.954
17	−77.545	$Pbca$	8	9.0119	10.1086	15.7254	90	90	90	176.7	179.0	0.948
18	−77.528	$P2_12_12_1$	4	7.4940	9.5999	9.8975	90	90	90	172.7	175.0	0.954
19	−77.521	$Pca2_1$	4	14.0252	5.9666	8.6201	90	90	90	178.6	179.7	0.941
20	−77.519	$P2_1/m$	2	5.1519	7.9480	8.7857	90	91.620	90	180.0	180.0	0.944
21	−77.496	$P2_1/c$	4	5.2019	15.5747	9.0339	90	101.534	90	175.8	178.5	0.947
22	−77.484	$Pna2_1$	4	11.3552	7.7651	8.1010	90	90	90	174.7	171.6	0.951
23	−77.457	$P2_1/c$	4	5.9462	14.0395	8.6425	90	90.211	90	174.8	176.6	0.941
24	−77.445	$Pna2_1$	4	15.0687	8.1922	5.7410	90	90	90	174.3	174.7	0.958
25	−77.440	$P\bar{1}$	4	5.1580	11.7462	11.8555	92.272	91.954	93.264	174.7	178.3	0.948
26	−77.432	$Pna2_1$	4	8.5392	9.6308	8.7737	90	90	90	178.8	178.0	0.941
27	−77.431	$P2_1$	2	5.9758	8.0994	7.6772	90	106.781	90	171.3	172.2	0.954
28	−77.336	$P2_1/m$	2	5.1590	7.7612	9.2291	90	103.166	90	180.0	180.0	0.943
29	−77.330	$P\bar{1}$	2	5.2388	7.7219	9.0372	86.641	80.518	80.323	169.1	173.6	0.956
30	−77.286	$P2_1/c$	4	5.1821	17.9322	7.8734	90	100.989	90	175.5	177.1	0.945
31	−77.281	$P\bar{1}$	4	7.5478	9.6313	10.1645	87.207	75.531	89.339	177.7	178.6	0.950
32	−77.271	$P2_1/c$	4	7.5360	9.6475	11.0255	90	116.971	90	179.9	178.7	0.950
33	−77.267	$P2_1/c$	8	9.2397	8.3830	18.6699	90	97.878	90	179.1	175.2	0.948

In order to fully include the molecular flexibility, all low-energy structures (excluding duplicates) were post-optimized with the program *Materials Studio* 4.4 (Accelrys Software Inc., 2008) using the Dreiding/X6 force field for intermolecular as well as intramolecular interactions. In a first step the calculations were performed without symmetry constraints, *i.e.* in *P*1 with the corresponding number of molecules per unit cell. Subsequently, all structures were checked for symmetry and transformed into the corresponding space group. For most structures the symmetry was the same as before the optimization; however, in some cases a reduced symmetry was observed (*e.g.* $P2_1/c$, $Z = 8$, rather than $C2/c$, $Z = 8$).

Finally the structures were optimized in the corresponding space groups and sorted again according to energy.

2.2. Results

The calculated low-energy structures are listed in Table 2 [atomic coordinates are given in the supplementary material; a plot of energies *versus* densities for all 304 structures within 5 kJ mol^{-1} above the global minimum is also included (Fig. S1)].

In all low-energy structures the ETBE adopts a *trans* conformation with $\tau_1 \simeq \tau_2 \simeq 180°$. Obviously this conformation is not only preferred in the gas phase, but also allows various energetically favourable packings in the solid state.

The best crystal structure energetically is found in the space group $P2_12_12_1$ ($Z = 4$) with the molecule in a general position. The molecule is almost exactly in the *trans* conformation with $\tau_1 = 177.1$ and $\tau_2 = 177.2°$.

3. Experimental determination of crystal structures

3.1. Experimental details

X-ray powder diffraction patterns were measured with Cu $K\alpha_1$ radiation in transmission mode on a Stoe Stadi-P diffractometer with a curved Ge(111) primary monochromator using a linear position-sensitive detector. All investigations were performed at low temperatures (80–160 K) with an Oxford Cryostream device. For the data acquisition the Stoe software *WinXPOW* (Stoe & Cie, 2005) was used.

Liquid ETBE was contained at room temperature in a glass capillary with 0.7 mm diameter and the capillary was sealed. For some samples the glass capillary was first filled with amorphous SiO_2 to reduce the preferred orientation. The samples were cooled rapidly by placing them under the cold-gas blower of the cryostream device and subsequently measured at constant temperature.

Low-temperature DSC measurements were performed on a DSC 131 (SETARAM). Liquid ETBE was weighed in

aluminium crucibles. The experiments were repeated ten times with different amounts of ETBE and different cooling and heating rates.
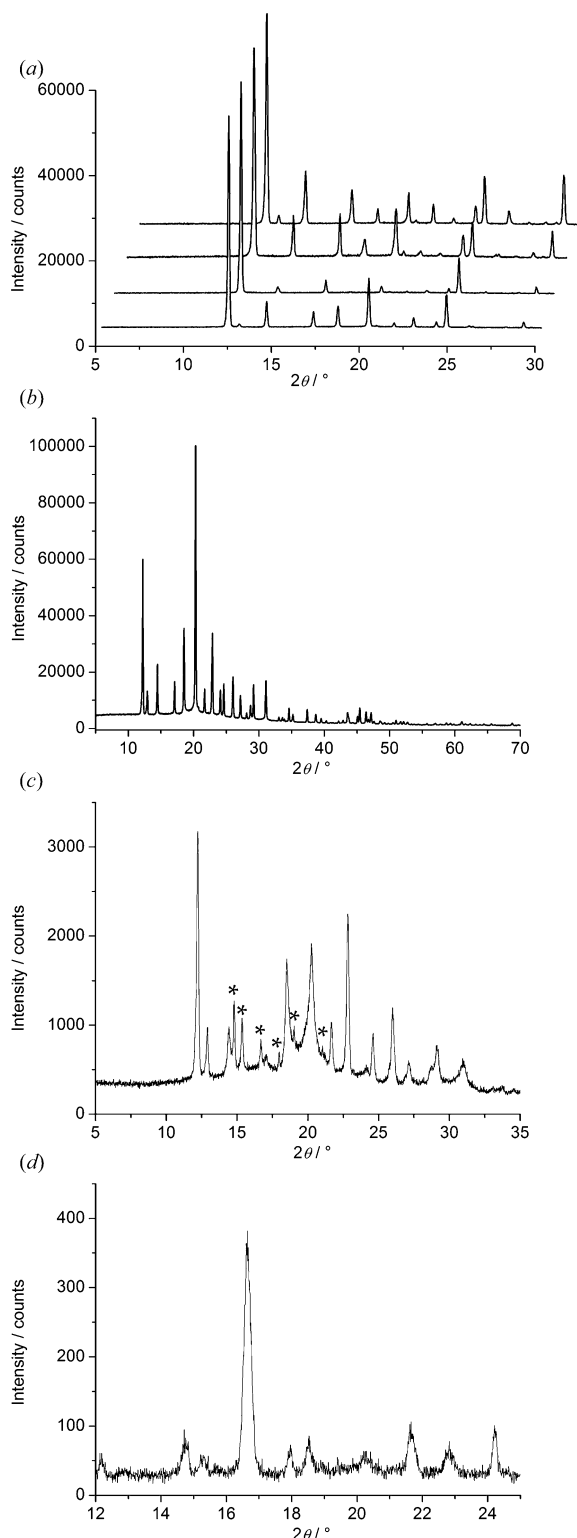
Figure 2
X-ray powder patterns of ETBE: (a) Typical samples of ETBE frozen in capillaries, showing the strong preferred orientation and texture effects; (b) sample with the reduced preferred orientation used for structure solution; (c) sample with admixtures of the β phase (reflections of the β phase are indicated by asterisks); (d) pure β phase with poor crystallinity.

3.2. Results

When ETBE is cooled below its melting point of 179 K it shows supercooling. In the DSC experiments the samples crystallized at temperatures of 151–168 K, depending on the amount of ETBE in the crucibles. Supercooling also occurred in the capillaries.

About 50 crystallization experiments were carried out in capillaries on the powder diffractometer. Single crystals could not be obtained. In all cases the ETBE formed a polycrystalline aggregate. The powder diagrams suffered from strong preferred orientation and texture effects (Figs. 2a–c). Finally we obtained one powder diffractogram with a reduced preferred orientation which was suitable for solving the crystal structure by real-space methods.

The powder data could be indexed using *DICVOL*91 (Boultif & Louër, 1991) within the *WinXPOW* software. From the 74 peaks used for the indexing only one very weak hump remained unindexed. The Figure of Merit F(30) was as high as 153.4. The indexing results in a C-centred monoclinic unit cell with lattice parameters of a = 14.7133 (14), b = 7.7597 (10), c = 6.2286 (7) Å, β = 100.999 (7)°, V = 698.07 (19) Å^3. According to volume increments (Hofmann, 2002) the unit cell should contain four molecules.

For the structure solution the powder pattern was truncated to a real space resolution of 1.4 Å, and the background was subtracted with a Bayesian high-pass filter (David & Sivia, 2001). At first a Pawley refinement was carried out with the program *DASH* (David *et al.*, 2006) using an asymmetry-corrected Voigt function. The systematically absent reflections led to the extinction symbol C 1–1, corresponding to the possible space groups $C2$, Cm and $C2/m$ (*International Tables for Crystallography*, 2002, Vol. A). The space group Cm with Z = 4 is very rare for organic compounds. Within the 503 348 organic crystal structures listed in the Cambridge Structural Database (Allen, 2002) by January 2010 there were nine structures with this symmetry. Hence we did not consider this space group further for ETBE. In $C2$, Z = 4, the molecules are situated in a general position; this symmetry has a frequency of $\sim$ 0.5%. In $C2/m$, Z = 4, the ETBE molecule must be situated on a mirror plane. $C2/m$ is a supergroup of $C2$, hence a structure in $C2/m$ should also be found during the calculations in $C2$.

The crystal structure was solved from powder diffraction data by real-space methods using simulated annealing with the program *DASH*. The molecular geometry was taken from Dreiding/X6 calculations. The torsion angles τ_1 and τ_2 were refined freely. First simulated annealing runs were made in $C2$. In the solutions the molecules adopted a *trans* orientation τ_1 = τ_2 = 180.0° and the molecular planes were perpendicular to [010], with molecules situated at y = 0 and y = 0.5; hence the resulting structures in fact showed the higher symmetry $C2/m$. Consequently, the final simulated annealing runs were performed in $C2/m$. The χ^2 profile was 3.92. The structures obtained in $C2$ were found again.

The crystal structure was refined by Rietveld methods using the program *TOPAS* (Coelho, 2007). At first, the background

Table 3
Crystallographic data of the Rietveld refined structure.

Crystal data	
Chemical formula	$C_6H_{14}O$
M_r	102.17
Crystal system, space group	Monoclinic, $C2/m$
Temperature (K)	123
a, b, c (Å)	14.7170 (3), 7.76462 (17), 6.22813 (16)
β (°)	101.0148 (15)
V (Å^3)	698.59 (3)
Z	4
Radiation type	Cu $K\alpha_1$, $\lambda = 1.54056$ Å
μ (mm^{-1})	0.49
Specimen shape, size (mm)	Cylinder, 10×0.7
Data collection	
Diffractometer	Stoe Stadi-P diffractometer
Specimen mounting	Glass capillary
Data collection mode	Transmission
Scan method	Step
2θ values (°)	$2\theta_{min} = 5.0$, $2\theta_{max} = 69.99$, $2\theta_{step} = 0.01$
Refinement	
R factors and goodness of fit	$R_p = 0.034$, $R_{wp} = 0.046$, $R_{exp} = 0.017$, $R_{Bragg} = 0.029$, $\chi^2 = 2.714$
No. of data points	6500
No. of parameters	114
No. of restraints	32
H-atom treatment	All H-atom parameters refined

Computer programs used: *WinXPOW* (Stoe & Cie, 2005), *TOPAS-Academic* (Coelho, 2007), *DASH* (David *et al.*, 2006), *Mercury* (Macrae *et al.*, 2008), *publCIF* (Westrip, 2010).

and the profile parameters were determined by a Pawley fit. The fit converged with an almost straight difference line and confidence values of $R_p = 0.025$ and $R_{wp} = 0.033$ (without background correction), $R'_p = 0.091$, $R'_{wp} = 0.102$ (with background correction) and $\chi^2 = 1.974$ (see Fig. S2 in the supplementary material).

The Rietveld refinements were carried out in $C2/m$ with the molecule fixed to the mirror plane. Restraints were used for all
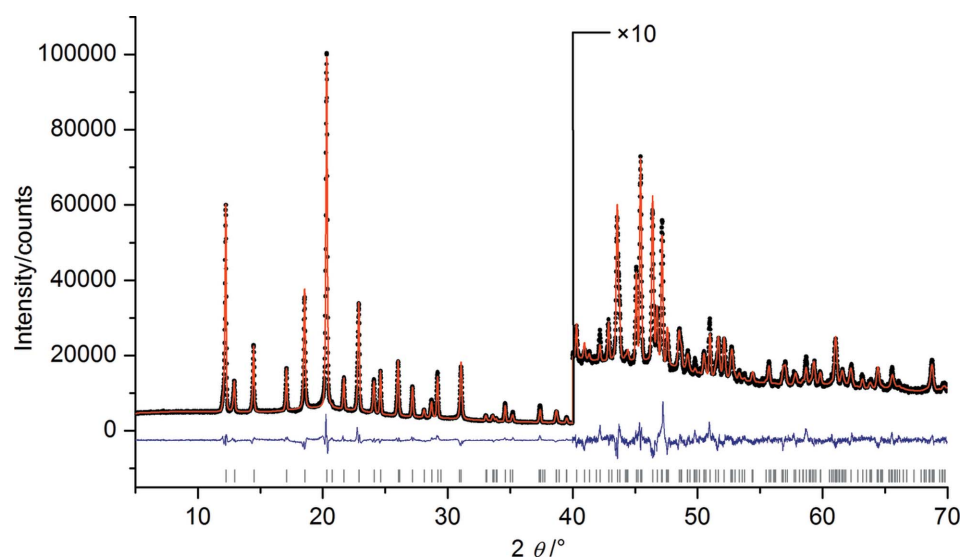
Figure 3
Rietveld plot of ETBE: experimental data are shown in black, calculated data are shown in red and the difference curve in blue. This figure is in colour in the electronic version of this paper.

bond lengths and angles. The atomic coordinates and lattice parameters were refined together with an overall isotropic displacement factor, scale factor, zero-point error, background and peak-profile parameters including anisotropic peak broadening. We tested for the preferred orientation. Although most samples had shown very strong preferred orientation effects, the sample used for structure solution and Rietveld refinement, to our astonishment, showed almost no preferred orientation. Nevertheless, a correction for preferred orientation in [111] improved the fit slightly.

The refinement converged with $R_p = 0.034$, $R_{wp} = 0.046$, $R'_p = 0.126$, $R'_{wp} = 0.146$ and $\chi^2 = 2.714$. The Rietveld plot is shown in Fig. 3. Crystallographic data are shown in Table 3. Atomic coordinates are given in the supplementary material.

ETBE crystallizes in $C2/m$ with $Z = 4$. The molecule adopts an exact *trans* conformation with $\tau_1 = \tau_2 = 180°$. The crystal structure is shown in Fig. 4. The molecules are situated on crystallographic mirror planes parallel to (010). In the [010] direction the molecules are stacked; within the stack neighbouring molecules are in an antiparallel orientation in order to avoid steric hindrance between the bulky *tert*-butyl groups (Fig. 4*b*). The shortest intermolecular distances within the stack are found between the O atom of one molecule and a *tert*-butyl group of a neighbouring molecule [O···C 3.732 (2) Å, O···H 2.678 (5) Å]. Within a stack the molecules are held together mainly by van der Waals interactions, supported by some Coulomb forces. Between neighbouring stacks there are van der Waals contacts only between C and H atoms.

3.3. On the polymorphism of ETBE

No reports of the possible polymorphism of ETBE were found in the literature.

The DSC measurements between 103 K and the melting point (179 K) did not give any indication of a phase transition or a second crystal phase.

However, in ~10 of the 50 recorded powder diagrams additional lines were visible which could not be indexed with the lattice of the refined crystal structures of ETBE. Obviously there is a second crystal phase, which we will call the β phase. This β phase could not be obtained reproducibly. In most cases the β phase occurred only as an admixture with the α phase (see Fig. 2*c*). We observed that the β content was only formed in those capillaries where firstly the α phase had been crystallized and subsequently melted. This is an indication that the formation of seeds may play a role. On the other hand, in some cases melting and cooling the capillary with a mixture of α

(a)

(b)
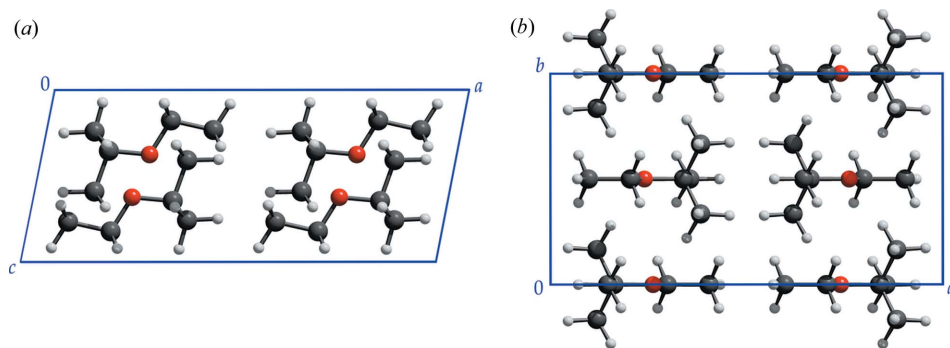
Figure 4
Refined crystal structure: (a) view direction [010]; (b) view direction [001].

and β phases led to the pure α phase without any additional lines. All these experiments confirmed that the additional lines were indeed caused by a second crystal phase of ETBE, and other explanations like impurities could be ruled out. The β phase is metastable; even at 123 K the phase disappeared completely after 3.5 h.

The β phase was obtained as a pure phase (as far as is visible) in only one experiment, but its crystallinity was very poor (see Fig. 2d). All attempts to obtain a better powder diagram of pure β phase failed. None of the powder diagrams of the β phase could be indexed in a reliable way and the structure could not be solved.

4. Discussion

Crystal structure prediction resulted in many structures with similar energies. Within a narrow energy range of only 2 kJ mol^{-1} above the global minimum, as many as 33 possible crystal structures were found. The structure with the highest density, i.e. with the most efficient molecular packing, of all the low-energy structures was found at energy rank 2, with an energy of only 0.54 kJ mol^{-1} above the global minimum. (This
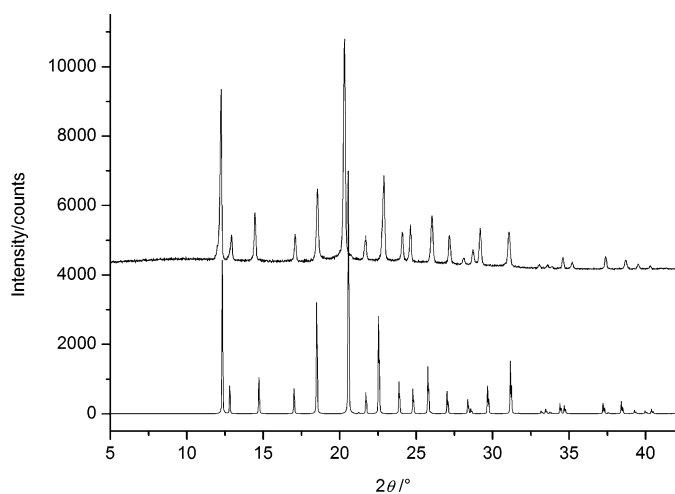
Figure 5
Comparison of the experimental X-ray powder diagram (top) with the simulated diagram of the predicted structure with energy rank 2 (bottom). There was no fit to the experimental data at this stage.

energy difference is far smaller than the accuracy of the method; if we had chosen a different set of atomic charges, the energetical order of the two structures would be reversed.) It is this dense structure which occurs experimentally and which was finally determined from X-ray powder data by real-space methods.

We actually obtained this structure with $C2/m$ symmetry from lattice-energy minimizations during an early stage of our investigations. We simulated its X-ray powder diagram and compared it to the experimental pattern. The peak positions matched, but the experimental patterns suffered so strongly from the preferred orientation and texture effects that the experimental peak intensities were not at all similar to those simulated from the predicted structure. All attempts at Rietveld refinements failed; neither was it possible to solve the structure by real-space methods from these powder data.

We had to continue the crystallization experiments until we obtained a powder pattern with reduced preferred orientation (which was similar to the simulated pattern, see Fig. 5); from this pattern the crystal structure could be solved by real-space methods and a reliable Rietveld refinement could be performed, which confirmed the predicted structure.

The differences between the predicted structure and the Rietveld-refined structure are below 0.12 Å in lattice parameters a, b, c, 1.7° in β, and on average 0.05 Å in the atomic coordinates of non-hydrogen atoms (see Fig. 6).

The corresponding methyl derivative, MTBE, crystallizes in $Pcab$ (which is a non-standard setting of $Pbca$) with molecules in general positions, $Z = 8$. Although the space groups differ for MTBE and ETBE, the structures have similarities: In MTBE the molecules adopt a $trans$ conformation ($\tau_1 = 179.7°$), as in ETBE. In MTBE the molecular planes do not coincide with crystallographic mirror planes, but nevertheless all the molecular planes are parallel. The MTBE molecules form stacks as in ETBE, with the $tert$-butyl groups avoiding contacts which are too close. In contrast to ETBE the stacks run in the [100] direction (rather than [010]) and there are four (instead of two) stacks per unit cell.

For ETBE a packing corresponding to the MTBE structure is found in the list of possible crystal structures with an energy of 8.425 kJ mol^{-1} above the global minimum. Hence, a MTBE-like arrangement would be very unfavourable for ETBE molecules.

The space group $C2/m$ for the ETBE structure is rare for molecular crystals. According to Kitaigorodskii (1961), neither the twofold axis nor the mirror plane allow for a dense packing of molecules.

A dense packing can only be achieved if the molecules themselves are situated on sites with m or $2/m$ symmetry. This was proven by Belsky et al. (1995): within 43 molecules crystallizing in $C2/m$, none were found in a general position, one in

a site with symmetry 2 and all others in m, $2/m$ or a combination of both.

In the CSD only 1% of all molecules occupy sites with symmetry m, and even amongst these structures, $C2/m$ is not a frequent space group. The space groups $Pnma$ ($Z = 4$), $P2_1/m$ ($Z = 2$) and $Cmc2_1$ ($Z = 4$) appear more frequently. The 4501 molecules of m symmetry in the CSD that are found occupying special positions of m symmetry are distributed over the space groups $Pnma$ (2324 structures), $P2_1/m$ (962 structures), $Cmc2_1$ (308 structures), $C2/m$ (212 structures), $Pbcm$ (145 structures), $Pmn2_1$ (130 structures) and other space groups (420 structures).

Why does ETBE crystallize with this uncommon symmetry? The answer was obtained from the lattice-energy calculations: For all structures with low energies, $C2/m$ allows the densest packing of ETBE molecules. The molecules are held together mainly by van der Waals interactions, supported by Coulomb interactions between the partially charged atoms.

For the β phase of ETBE we tried to solve the crystal structure by lattice-energy minimizations. For all low-energy structures powder diagrams were simulated and compared with the experimental powder patterns of the β phase. However, it was not possible to decide which of the calculated patterns corresponds to the experimental one, as the quality of the powder data of the β phase was too poor. Furthermore, the peak intensities were not reliable because of the strong preferred orientation.

Compounds which are liquid at room temperature may be crystallized not only by lowering the temperature but also by applying high pressure (Olejniczak, Katrusiak & Vij, 2009; Olejniczak, Katrusiak, Metrangoloand *et al.*, 2009; Gajda & Katrusiak, 2009; Dziubek *et al.*, 2009). In ETBE the α phase has – according to lattice-energy minimizations – a higher density than all the other low-energy structures. Hence, at high pressures the α phase will be even more stable and it is unlikely that the β phase could be better obtained under pressure.

5. Conclusion

This work shows the possibilities and the main limitations for solving crystal structures from X-ray powder data, either by real-space methods or by lattice-energy minimizations. The quality of the powder data is crucial. Real-space methods generally require the powder diagram to be indexed. Lattice-energy minimizations have also been proven to work with samples of low crystallinity and non-indexable powder diagrams showing only 8–12 peaks (Schmidt *et al.*, 2005; Paulus *et al.*, 2007). However, if the powder data suffer from very strong preferred orientation or texture effects (as shown in Figs. 2*a* and *b*), or if the phase is present only as a minor component in a mixture (Fig. 2*c*), or if the powder diagram consists of only 12 broad humps (Fig. 2*d*), it becomes impossible to select which of the calculated structures corresponds to the experimental pattern. Furthermore, it is difficult to prove whether the selected structure is the correct one because a Rietveld refinement will not give a reliable result (Buchsbaum & Schmidt, 2007). In such a case additional information is required, *e.g.* from spectroscopy, electron diffraction or pair-distribution function analysis.

References

Accelrys Software Inc. (2008). *Materials Studio* 4.4. Accelrys Software Inc., San Diego, CA.

Allen, F. H. (2002). *Acta Cryst.* B**58**, 380–388.

Belsky, V. K., Zorkaya, O. N. & Zorky, P. M. (1995). *Acta Cryst.* A**51**, 473–481.

Boultif, A. & Louër, D. (1991). *J. Appl. Cryst.* **24**, 987–993.

Buchsbaum, C. & Schmidt, M. U. (2007). *Acta Cryst.* B**63**, 926–932.

Coelho, A. A. (2007). *TOPAS Academic*, Version 4.1. Coelho Software, Brisbane, Australia.

David, W. I. F. & Sivia, D. S. (2001). *J. Appl. Cryst.* **34**, 318–324.

David, W. I. F., Shankland, K., van de Streek, J., Pidcock, E., Motherwell, W. D. S. & Cole, J. C. (2006). *J. Appl. Cryst.* **39**, 910–915.

Dziubek, K., Podsiadło, M. & Katrusiak, A. (2009). *J. Phys. Chem. B*, **113**, 13195–13201.

EFOA (2005). *The European Fuel Oxygenates Association MTBE Resource Guide*, Version 3, 2nd revision. EFOA, Brussels, Belgium.

Egawa, T., Moriyama, H., Takeuchi, H., Konaka, S., Siam, K. & Schäfer, L. (1993). *J. Mol. Struct.* **298**, 37–45.

Frisch, M. J. *et al.* (2004). *GAUSSIAN*03, Revision B.01. Gaussian Inc., Wallingford, CT, USA.

Hofmann, D. W. M. (2002). *Acta Cryst.* B**58**, 489–493.

Gajda, R. & Katrusiak, A. (2009). *J. Phys. Chem. B*, **113**, 2436–2442.

Gasteiger, J. & Marsili, M. (1980). *Tetrahedron*, **36**, 3219–3222.

Kalkhof, K. (2002). PhD Thesis. Technical University of Darmstadt, Germany.

Kitaigorodskii, A. I. (1961). *Organic Chemical Crystallography*, pp. 94–101. New York: Consultants Bureau.

Macrae, C. F., Bruno, I. J., Chisholm, J. A., Edgington, P. R., McCabe, P., Pidcock, E., Rodriguez-Monge, L., Taylor, R., van de Streek, J. & Wood, P. A. (2008). *J. Appl. Cryst.* **41**, 466–470.
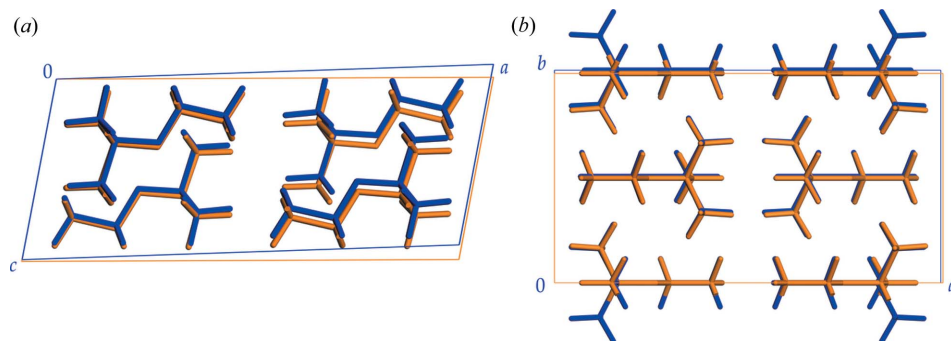
Figure 6
Comparison of the crystal structure determined from X-ray powder data (orange) and the structure predicted by lattice-energy minimization with rank 2 (blue). (*a*) View direction [010]; (*b*) view direction [001]. This figure is in colour in the electronic version of this paper.

research papers

Mayo, S. L., Olafson, B. D. & Goddard, W. A. III (1990). *J. Phys. Chem.* **94**, 8897–8909.

Olejniczak, A., Katrusiak, A., Metrangolo, P. & Resnati, G. (2009). *J. Fluorine Chem.* **130**, 248–253.

Olejniczak, A., Katrusiak, A. & Vij, A. (2009). *CrystEngComm*, **11**, 1073–1080.

Paulus, E. F., Leusen, F. J. J. & Schmidt, M. U. (2007). *CrystEngComm*, **9**, 131–143.

Schmidt, M. U., Ermrich, M. & Dinnebier, R. E. (2005). *Acta Cryst.* B**61**, 37–45.

Schmidt, M. U. & Kalkhof, H. (2002). *CRYSCA*. Frankfurt am Main, Germany.

Slovokhotov, Yu. L., Timofeeva, T. V., Antipin, M. Yu. & Struchkov, Yu. T. (1984). *J. Mol. Struct.* **112**, 127–140.

Steininger, R., Bilgram, J. H., Gramlich, V. & Petter, W. (1989). *Z. Kristallogr.* **187**, 1–13.

Stoe & Cie (2005). *WinXPOW*, Version 2.23. Stoe & Cie, Darmstadt, Germany.

Suenram, R. D., Lovas, F. J., Pereyra, W., Fraser, G. T. & Walker, A. R. H. (1997). *J. Mol. Spectrosc.* **181**, 67–77.

Wezel, A. van, Puijker, L., Vink, C., Versteegh, A. & de Voogt, P. (2009). *Chemosphere*, **76**, 672–676.

Westrip, S. P. (2010). *J. Appl. Cryst.* **43**, 920–925.